

A network of phosphate starvation and immune-related signaling and metabolic pathways controls the interaction between *Arabidopsis thaliana* and the beneficial fungus *Colletotrichum tofieldiae*

Henning Frerigmann^{1,2}, Markus Piotrowski³, René Lemke³, Paweł Bednarek^{2*}, Paul Schulze-Lefert^{1*}

¹ Max Planck Institute for Plant Breeding Research, Department of Plant Microbe Interactions and Cluster of Excellence on Plant Sciences (CEPLAS), D-50829 Cologne, Germany

² Institute of Bioorganic Chemistry, Polish Academy of Sciences, 61-704 Poznań, Poland

³ Lehrstuhl für Molekulargenetik und Physiologie der Pflanzen, Ruhr-Universität Bochum, D-44801 Bochum, Germany

* Corresponding authors: schlef@mpipz.mpg.de; bednarek@ibch.poznan.pl

Abstract

The beneficial root-colonizing fungus *Colletotrichum tofieldiae* (*Ct*) mediates plant growth promotion (PGP) upon phosphate (Pi) starvation in *Arabidopsis thaliana* (*Arabidopsis*). This activity is dependent on the Trp-metabolism of the host, including indole glucosinolate (IG) hydrolysis. Here we show that *Ct* resolves several Pi starvation-induced molecular processes in the host, one of which is the downregulation of auxin signaling in germ-free plants, which is restored in the presence of the fungus. Using CRISPR/Cas9 genome editing, we generated an *Arabidopsis* triple mutant lacking three homologous nitrilases (NIT1-3) that are thought to link IG-hydrolysis products with auxin biosynthesis. Retained *Ct*-induced PGP in *nit1;2;3* mutant plants demonstrated that this metabolic connection is dispensable for the beneficial activity of the fungus. This suggests that either there is an alternative metabolic link between IG-hydrolysis products and auxin biosynthesis, or that *Ct* restores auxin signaling independently of IG metabolism. We show that *Ct*, similar to pathogenic microorganisms, triggers *Arabidopsis* immune pathways that rely on IG metabolism as well as salicylic acid and ethylene signaling. Analysis of IG-deficient *myb* mutants revealed that these metabolites are indeed important for control of *in planta Ct* growth: however, enhanced *Ct* biomass does not necessarily negatively correlate with PGP. We show that Pi deficiency enables more efficient colonization of *Arabidopsis* by *Ct*, possibly due to the MYC2-mediated repression of ethylene signaling and changes in the constitutive IG composition in roots.

Key words: beneficial fungi, plant growth promotion, phosphate availability, auxin, indole glucosinolates

Introduction

Because of its low availability and mobility phosphate (Pi) is frequently limiting for plant growth and yield. Plants have evolved to cope with limited Pi availability by developing different adaptive mechanisms collectively known as the Pi starvation response (PSR). Activation of the PSR is dependent on a number of different signaling molecules including plant hormones, sugars, peptides, and reactive oxygen species, and is controlled by phosphate starvation response (PHR)-transcription factors (Chien et al., 2018; Crombez et al., 2019). The PSR brings about modifications of the root system architecture, including inhibition of primary root growth, and enhanced lateral root development and root hair formation, which collectively enable more efficient Pi foraging (Péret et al., 2011). These modifications in root architecture are controlled by local changes in auxin levels and auxin sensitivity that are induced by Pi starvation (Bates and Lynch, 1996; Nacry et al., 2005; Pérez-Torres et al., 2008).

The efficiency of Pi foraging can be further increased by conserved symbiotic associations with arbuscular mycorrhizal fungi, whose hyphae can serve as an extension of the plant root system (Parniske, 2008). Despite the benefits of association with mycorrhizal fungi, about 30% of plant species, including the Brassicaceae family, have lost the ability to form this symbiotic interaction (Cosme et al., 2018). Experimental evidence, however, suggests that other beneficial microorganisms support such plants in increasing Pi acquisition ability. For instance, the endophytic fungus *Colletotrichum tofieldiae* has been found to promote the growth of the model plant *Arabidopsis thaliana* (*Arabidopsis*) under low Pi availability (50 μ M), and of tomato and maize under ample Pi supply (Hiruma et al., 2016; Díaz-González et al., 2020). The beneficial outcome of this interaction has been reported to be independent from signaling activated by the phytohormones jasmonate, ethylene, and salicylic acid, but requires the intact PENETRATION2 (PEN2) pathway for indole glucosinolate (IG) metabolism (Bednarek et al., 2009; Hiruma et al., 2016). Glucosinolates are amino acid-derived thioglucosides that are produced constitutively by species from the Brassicales order (Halkier and Gershenzon, 2006). These specialized metabolites have been shown to contribute to protecting Brassicales plants from different pests, including herbivorous insects and pathogenic microorganisms (Hopkins et al., 2009; Pastorczyk and Bednarek, 2016). Intact glucosinolates are not biologically active; however, hydrolysis of these metabolites by β -thioglucosidases (myrosinases) results in the formation of a number of chemically-reactive and biologically active metabolites (Wittstock et al., 2016).

In *Arabidopsis*, glucosinolates are biosynthesized primarily from methionine (aliphatic glucosinolates; AGs) and from tryptophan (IGs). The two classes of glucosinolates differ not only in their precursor and side chain structure, but also in their biological functions. For instance IGs, but not AGs, are metabolized by the PEN2 myrosinase to control entry of

different filamentous pathogens into leaf epidermal cells (Pastorczyk and Bednarek, 2016). In addition to PEN2, IG function in immunity is dependent on the CYP81F2 P450 monooxygenase that hydroxylates unsubstituted indol-3-ylmethyl glucosinolate (I3M) to form 4-hydroxy-I3M, which is converted by a cognate O-methyltransferase to 4-methoxy-I3M (4MO-I3M) (Bednarek et al., 2009; Clay et al., 2009; Pfalz et al., 2011). Apart from their functions in defense, IGs are also implicated in auxin homeostasis (Malka and Cheng, 2017). It has been shown that indole-3-acetonitrile (IAN), one of the products of myrosinase-mediated I3M hydrolysis, can be converted by nitrilases (NITs) from the Brassicaceae-specific NIT1-subfamily into indole-3-acetic acid (IAA), which is the simplest and most abundant form of auxin (Fig. 1) (Normanly et al., 1997; Vorwerk et al., 2001; Lehmann et al., 2017).

The first step in IG biosynthesis is catalyzed by two redundant P450 monooxygenases, CYP79B2 and CYP79B3, which convert tryptophan into indole-3-acetaldoxime (IAOx) (Zhao et al., 2002). In addition to IGs, this intermediate is also a precursor of other specialized indole-type metabolites, including the phytoalexin camalexin and indole-3-carboxylic acid derivatives, which are all important for Arabidopsis immunity (Fig. 1) (Glawischnig et al., 2004; Böttcher et al., 2014; Pastorczyk et al., 2020). Consequently, *cyp79b2 cyp79b3* double mutant plants, which are depleted of all these Trp-derivatives, are highly susceptible to many filamentous plant pathogens (Sanchez-Vallet et al., 2010; Hiruma et al., 2013). Moreover, these plants are no longer able to establish beneficial interactions with *Ct*, which behaves as a pathogen in this genetic background (Hiruma et al., 2016).

In this study, we investigated the molecular basis underpinning *Ct*-induced plant growth promotion (PGP) under low Pi levels in Arabidopsis. Our results indicated that *Ct*-induced PGP strictly correlates with reversion of the PSR. We show that colonization of Arabidopsis roots with *Ct* induces changes in auxin signaling, but that the biosynthetic link between IGs and IAA is not critical for the outcome of this interaction. Finally, we show that despite its beneficial effects, *Ct* induces immune-related salicylic acid- and ethylene-dependent responses, as well as IG biosynthesis.

Results

Phosphate availability and light intensity influence *Ct*-dependent PGP

We tested *Ct*-induced PGP in Arabidopsis plants grown on an agar matrix using a normal level of inorganic phosphate (Pi) supply (625 μ M Pi), and two different phosphate starvation conditions (100 and 50 μ M Pi, representing moderate and severe phosphate deficiency, respectively) under the illumination of 11250 lx. As reported previously, *Ct* colonization did not increase shoot fresh weight under normal phosphate supply. Strikingly, fungal

colonization also failed to increase shoot biomass when plants were grown on 50 μM Pi (Fig. 2A). A statistically significant increase in shoot fresh weight in *Ct*-colonized plants, compared to controls, was observed only when plants were grown on medium containing 100 μM Pi (Fig. 2A). Thus in our experimental system, *Ct* has a clear impact on shoot biomass only under moderate phosphate deficiency. In contrast to the concentration-dependent changes in plant fresh weight, we observed a statistically significant *Ct*-triggered increase in plant root length under all tested Pi concentrations (Fig. 2B). To check if PGP correlates with *in planta* fungal growth, we estimated *Ct* biomass in colonized plant tissue by quantifying fungal *TUBULIN2* (*CtTUB2*) in DNA samples isolated from roots of colonized plants. This analysis indicated that fungal biomass was significantly increased in plants grown on media containing 100 μM Pi, as compared with 625 μM Pi (Supplementary Fig. S1). When plants were grown on 50 μM Pi, we found a greater variation in fungal biomass between the root replicates, which was not significantly different compared to plants grown on 100 μM Pi. Therefore, there is no correlation between the extent of *Ct* root colonization and PGP at 100 and 50 μM Pi.

To check if *Ct*-mediated PGP can also be affected by light conditions, we repeated the same experiment with plants growing under lower light intensities (3600 and 6800 lx). Subsequent analysis indicated that the relative difference in shoot fresh weight between plants grown under normal or limited Pi decreases with reduced light intensity (Supplementary Fig. S2). Despite this, we were still able to observe statistically significant *Ct*-mediated PGP activity when plants were grown on 100 μM Pi under 3600 and 6800 lx. In contrast to higher light intensities, the lowest light intensity tested induced a significant increase in shoot fresh weight, even in plants grown on 50 μM Pi. Overall, this result indicated that in addition to Pi levels, PGP is also affected by light conditions. Since the highest tested light intensity resulted in the highest fold-change in shoot fresh weight, we decided to conduct subsequent experiments under this condition.

Phosphate starvation-induced IAA depletion is reverted by *Ct* colonization

Pi starvation induces auxin signaling, which can lead to increased root hair formation (Bates and Lynch, 1996; Nacry et al., 2005; Pérez-Torres et al., 2008). We observed that *Ct*-mediated colonization of *Arabidopsis* plants grown on 100 μM Pi increased the number and length of root hairs (Supplementary Fig. S3). This suggested that under Pi-deficient conditions, *Ct* may have an impact on auxin accumulation or auxin signaling. To test this hypothesis, we decided to perform our experiments using a transgenic line expressing GUS, under the control of the auxin-responsive DR5 synthetic promoter (Ulmasov et al., 1997). Our analysis revealed a clear reduction in total GUS activity in samples obtained from intact *DR5::GUS* seedlings grown on 100 μM Pi, as compared with 625 μM Pi. An additional

significant drop in GUS activity was observed in seedlings grown on 50 μM Pi (Fig. 3). These results showed that phosphate starvation significantly dampens auxin accumulation in a dose-dependent manner, indicating lower IAA levels under these conditions. Colonization of roots with *Ct* under sufficient Pi supply did not affect GUS activity; however, colonization of roots grown on Pi-deficient media restored GUS activity to the levels observed in plants grown on normal Pi supply (Fig. 3). Overall, these results revealed that the negative impact of phosphate starvation on IAA signaling can be reverted by colonization with *Ct*.

Trp-metabolism, but not NIT1-subfamily members, influences the interaction between *Ct* and Arabidopsis

The PEN2 myrosinase has been reported to be required for *Ct*-triggered PGP. We thus hypothesized that the observed *Ct*-induced increase in IAA signaling could be linked to PEN2-mediated IG metabolism (Hiruma et al., 2016). To examine this possibility, we decided to investigate the requirement of three nitrilases (NIT1-3) from the Brassicaceae-specific NIT1-subfamily, which are thought to catalyze the conversion of I3M-derived indole-3-acetonitrile (IAN) into IAA (Fig. 1) for *Ct*-induced PGP. *NIT2*, *NIT1* and *NIT3* are organized as a gene cluster on chromosome III (Hillebrand et al., 1998), which hinders the generation of double- and triple-knockout lines by crossing respective single mutant plants. We therefore generated a $\Delta\text{NIT1/NIT2/NIT3}$ triple knockout line using CRISPR/Cas9. In addition, we used a line in which the expression of *NIT1* and *NIT2* genes is diminished by RNA interference (hereafter referred to as *NIT2 RNAi*) (Lehmann et al., 2017). Using these generated lines, we determined the role of IG metabolism in *Ct*-induced PGP. In these experiments we also used the *pen2* knockout, IG-deficient *myb34 myb51 myb122* (*myb-tr*) triple mutant, and the *cyp79b2 cyp79b3* (*cyp79b2b3*) double mutant that is deficient in all IAOx-derived secondary metabolites. Among all the tested lines, the most striking effect on plant growth was observed in the *cyp79b2b3* plants. In this case, growth of about 95% of *Ct*-inoculated seedlings ceased with fungal overgrowth, detectable already at the very early developmental stages. The seedlings that survived this stage and remained alive at the age of four weeks were not only significantly smaller than the *Ct*-colonized WT plants, but were also smaller in size than the respective MOCK-treated plants (Fig. 4CD). In addition, *cyp79b2b3* was the only tested line in which colonization with *Ct* did not increase root length (Fig. 4AB). Overall, this result indicated that lack of IAOx-derived metabolites not only interferes with *Ct*-induced PGP, but also leads to an additional growth penalty during interaction with *Ct*. As indicated by our qPCR analysis, this growth defect clearly correlated with increased *Ct* biomass in the surviving *cyp79b2b3* mutant plants, as compared with WT plants (Fig. 5A). Other tested mutants, including $\Delta\text{NIT1/2/3}$ and *NIT2 RNAi*, were not defective in the *Ct*-induced PGP (Fig. 4D). *myb-tr* and *pen2* mutations resulted in slight, but significant reductions in the length of

Ct-colonized roots on 100 μ M Pi (Fig. 4B). Notably, although PGP was WT-like, the *myb-tr* mutation led to elevated *Ct* biomass in colonized plants grown on 100 μ M Pi (Fig. 5A), suggesting that increased fungal growth does not necessarily negatively affect plant performance.

Although there was no clear reduction in shoot fresh weight, we observed that some of the *Ct*-inoculated *pen2* and *myb-tr* seedlings did not survive the early stages of development, similar to many of the *cyp79b2b3* seedlings. To estimate the contribution of these non-surviving seedlings to plant yield, we measured total dry weight of seedlings per plate (Fig. 5B). This indicated a significant drop in the total dry weight of *pen2* and *myb-tr*, as compared with WT seedlings. However, similar to the shoot fresh weight, we did not observe any differences between WT and Δ *NIT1/2/3* or *NIT2 RNAi* plants (Fig. 5).

Prompted by the lack of growth defects in tested nitrilase mutants, we checked how Pi levels and interaction with *Ct* affect expression of the three members of the *NIT1*-subfamily. Earlier RNAseq analysis performed in a similar experimental system as used in this study indicated that Pi level does not significantly affect expression of these three genes in roots, while *NIT1* expression is downregulated during colonization with *Ct* (Hacquard et al., 2016). Our RT-qPCR analysis of samples prepared from whole seedlings revealed that *NIT1* expression is neither significantly affected by Pi concentrations, nor by plant colonization with *Ct* (Fig. 6A). In contrast to *NIT1*, expression of *NIT2* and *NIT3* was significantly increased by Pi starvation in intact seedlings and this increase was reversed by *Ct* colonization (Fig. 6BC). Together, these results negatively correlated with the observed changes in GUS activity in *DR5::GUS* plants (Fig. 3), suggesting that *NIT1/NIT2/NIT3* are dispensable for the reversion of IAA accumulation in *Ct*-colonized roots. Overall, our analyses as well as earlier results (Hacquard et al., 2016) do not support a link between NIT-mediated conversion of I3M to IAA, and *Ct*-induced PGP.

Impact of *Ct* on indole glucosinolate accumulation resembles that of plant pathogens

To obtain more detailed insight into the function of glucosinolates in the PGP we investigated how Pi availability and interaction with *Ct* affects accumulation of these compounds. Our HPLC analysis revealed that Pi deficiency significantly increases total AG and IG accumulation in shoots (Fig. 7A). The observed change in total IG levels was associated with elevated accumulation of all compounds included in this group (Fig. 7B). In contrast to shoots, in roots Pi deficiency did not affect the accumulation of AGs (Fig. 7C). In this organ, we also did not observe any significant differences between IG levels at 625 and 100 μ M Pi. Only at a Pi level of 50 μ M did we observe slightly reduced total IG levels, which was specifically associated with a drop in the accumulation of 4MO-I3M and, particularly, 1MO-I3M (Fig. 7CD).

Our analysis did not reveal any clear impact of *Ct* colonization on AG accumulation in shoots and roots (Fig. 7AC). However, colonization with the fungus under Pi-deficient conditions had a significant impact on IG levels, particularly on the accumulation of 4MO-I3M, which was induced by *Ct* in roots and shoots of plants grown on 100 and 50 μM Pi (Fig. 7). In addition, we observed a significant reduction of I3M levels in shoots of colonized plants grown on 100 μM Pi, as compared with the respective MOCK samples. Unlike I3M and 4MO-I3M, 1MO-I3M levels were not affected by *Ct* colonization (Fig. 7BD). Overall, the observed *Ct*-induced changes in IG accumulation resembled those reported in pathogen-inoculated leaves (Pastorczyk and Bednarek, 2016), suggesting that the IG biosynthetic pathway responds similarly to pathogenic and beneficial fungi.

Colonization of Arabidopsis with *Ct* reverts PSR and induces immune responses.

Our analysis revealed that colonization with *Ct* can revert, completely or partially, Pi deficiency-induced changes in IAA signaling, and *NIT2* and *NIT3* expression in intact seedlings (Fig. 3, Fig. 6BC). For this reason, we decided to test whether colonization with *Ct* can generally revert the phosphate starvation response (PSR) in Arabidopsis. To this end, we investigated the expression profile of the Pi starvation marker genes, including two noncoding RNAs *IPS1* and *miR399D* (Fujii et al., 2005; Franco-Zorrilla et al., 2007), and *AtPT1*, which encodes a phosphate transporter (Muchhal et al., 1996). As shown by Hacquard et al., (2016), the expression of *IPS1*, but not of *miR399D* and *AtPT1*, can be significantly downregulated in roots during *Ct* colonization under low Pi levels. Our RT-qPCR analysis performed on RNA samples isolated from intact seedlings indicated that both of the noncoding RNAs were upregulated at 100 and 50 μM Pi, while the expression of *AtPT1* was upregulated only at 50 μM as compared with 625 μM Pi (Fig. 6DEF). Of note, colonization with *Ct* partially reverted transcriptional activation not only of *IPS1*, but also of *miR399D* at 50 μM Pi (Fig. 6DE). However, similarly to Hacquard et al. (2016), we did not observe a clear impact of *Ct* colonization on *AtPT1* expression (Fig. 6F).

As Pi-deficiency induces the jasmonate signaling pathway (Khan et al., 2016), we became interested in the expression of the jasmonate-responsive gene *VSP2*, and of *PDF1.2*, which is activated synergistically by both jasmonate and ethylene (Liu et al., 2005; Zarei et al., 2011). In contrast to the analysis performed in roots (Hacquard et al., 2016), we found that in intact seedlings the expression of *VSP2* was clearly enhanced under Pi deficiency, which confirms activation of jasmonate signaling under our experimental conditions (Fig. 6I). Moreover, in accordance to the behavior of the tested PSR markers, this was reverted in the presence of *Ct* (Fig. 6I). In contrast to *VSP2*, expression of *PDF1.2* was significantly downregulated at 50 μM Pi, as compared to 625 μM Pi (Fig. 6H). The presence of *Ct* not only reverted *PDF1.2* expression to the levels observed under normal Pi supply, but

strongly upregulated expression of this marker gene under all tested Pi concentrations. Interestingly, *PDF1.2* expression was below the detection limit in roots, despite Pi-limiting conditions and *Ct* colonization (Hacquard et al., 2016), suggesting that the changes in expression of this gene observed in our analysis (Fig. 6H) occur predominantly in leaves. The upregulation of *PDF1.2* could be mediated by an increase in ethylene levels resulting from the defense response triggered by *Ct*. In accordance with this assumption, we observed that *Ct* colonization abolished Pi starvation-triggered anthocyanin accumulation in leaves, which has been reported to be negatively regulated by ethylene (Lei et al., 2011), as well as positively by jasmonate (Khan 2016) (Supplementary Fig. S4). Finally, we determined expression of the *PR1* gene, which is a marker of the salicylic acid signaling pathway. Similar to *PDF1.2*, expression of this gene was below the detection limit in roots under analogous experimental conditions (Hacquard et al., 2016). Our analysis carried out with samples prepared from intact seedlings indicated that expression of *PR1* was clearly upregulated in response to Pi deficiency, which could reflect the reported impact of Pi availability on the accumulation of salicylic acid (Pant et al., 2015; Prerostova et al., 2018). However, instead of reverting *PR1* transcription, co-cultivation with *Ct* led to a further significant increase in the expression of this gene, indicating that salicylic acid-dependent immune responses are induced during the interaction with *Ct*. Overall, our analysis revealed that colonization with *Ct*, at least partially, reverts PSR-related signaling in Arabidopsis. However, in the case of SA and ethylene signaling pathways that are involved both in the response to Pi starvation and in plant immunity, this reversion overlaps with *Ct*-mediated induction of the expression of the respective genes.

Discussion

In this study we investigated the molecular mechanism underlying *Ct*-induced PGP in Arabidopsis. Our results indicate that colonization of Arabidopsis plants with *Ct* under Pi-deficient conditions resolves the PSR. This PSR resolution is characterized by a downregulation of two Pi starvation-responsive noncoding RNAs *IPS1* and *miR399D*, the jasmonate-responsive *VSP2* gene, and *NIT2* and *NIT3*, observed in intact seedlings (Fig. 6BCDEI). Considering a similarly significant reversion of gene expression was observed in roots only for *IPS1* (Hacquard et al., 2016), interestingly, this phenomenon also occurs in leaves that are not directly associated with *Ct*. In addition, colonization with *Ct* restored IAA signaling in plants grown under low Pi availability (Fig. 3). Resolution of the PSR response corresponded with PGP in plants grown at moderate (100 μ M) Pi, but not at severe (50 μ M) Pi deprivation. As exemplified for *IPS1* expression, the observed lack of PGP at the lower Pi concentration correlated with a stronger PSR response as compared to plants grown at moderate Pi, which was not always completely reverted by *Ct*. Additionally, the expression of

AtPT1 was higher at severe compared with moderate Pi deficiency, and this change was not significantly reverted by *Ct* colonization. In contrast to the differences in PGP and in the PSR markers, we did not observe significant changes in the *Ct* biomass between moderate and severe Pi deprivation (Supplementary Fig. S1), indicating that the capacity of Arabidopsis to control *Ct* growth *in planta* is similar at both tested Pi concentrations. Overall, these findings suggest that lack of PGP at 50 μ M Pi results from a stronger Pi deficiency that could not be fully compensated for by the interaction with *Ct*, rather than from fungal overgrowth that could negatively impact plant growth under this specific condition. Thus, within the tested Pi gradient (625, 100 and 50 μ M), beneficial activity of *Ct* on Arabidopsis growth under our experimental conditions is limited to a Pi stress optimum. Consequently, *Ct*-mediated PGP is not observed at both extremes of the gradient.

In addition to the expression of PSR markers, Pi deficiency has a strong impact on the biosynthesis of glucosinolates. This was particularly obvious in the shoots of tested plants, which accumulated significantly higher amounts of AGs and IGs (Fig. 7A). These elevated glucosinolate levels are in accordance with an earlier study that revealed enhanced accumulation of selected glucosinolates in shoots and roots of Arabidopsis plants grown under phosphate deficiency (Pant et al., 2015). However, this inverse relationship between Pi status and glucosinolate accumulation is not unique for these compounds, as it was also observed for other secondary metabolites including different types of phenylpropanoids. In contrast to the study of Pant et al. (2015), in our experiments total glucosinolate levels were only weakly affected in roots, suggesting that in addition to Pi deficiency, other factors are necessary to increase glucosinolate accumulation in this organ. The biological significance of elevated accumulation of different types of metabolites, including glucosinolates, under Pi starvation remains unclear. It has been shown that these changes are mediated predominantly by the MYB transcription factor PHOSPHATE STARVATION RESPONSE 1 (PHR1) with minor, if any, contribution of the E2 conjugase PHOSPHATE2 and *miR399* (Pant et al., 2015). However, as the *phr1* mutant still benefited from colonization with *Ct* under Pi starvation (Hiruma et al., 2016), the observed Pi-dependent changes in secondary metabolite accumulation seem to be dispensable for PGP under these conditions.

Our experiments indicate that apart from the Pi status, accumulation of IGs is also affected during the interaction with *Ct* (Fig. 7). These changes mirror those observed during colonization of Arabidopsis leaves with biotrophic and necrotrophic fungal pathogens, and include elevated accumulation of 4MO-I3M, the formation of which is mediated by the CYP81F2 monooxygenase and cognate methyltransferases (Bednarek et al., 2009; Pfalz et al., 2011; Pastorczyk and Bednarek, 2016). This is also in accordance with an earlier study on the interaction of Arabidopsis with the sebacinoid root-associated fungi *Piriformospora indica* and *Sebacina vermifera* (Lahrmann et al., 2015). Collectively, these observations

suggest similarities between the mechanisms of IG metabolism involved in controlling the growth of pathogenic and beneficial microorganisms. In line with this assumption, analysis of PGP and *Ct* biomass in a series of mutants defective in Trp and IG metabolism indicated that the end products of these pathways are synergistically controlling the impact of *Ct* on *Arabidopsis* growth, as well as *in planta* development of this fungus (Fig. 4, 5) (Hiruma et al., 2016). In this context, it is instructive that Pi starvation reduced the accumulation of 4MO-I3M in roots (Fig. 7D), suggesting that under Pi deficiency plants curtail constitutive chemical defense to increase the chance of colonization with a beneficial root-colonizing microbe, which could help the host acquire this nutrient. However, analysis of the *cyp81f2* mutant plants revealed that, in contrast to the interaction with leaf-infecting pathogens, CYP81F2 is not essential for limiting colonization of *Arabidopsis* with *P. indica* and *S. vermifera* (Lahrmann et al., 2015). This suggests that 4MO-I3M is dispensable for controlling the growth of beneficial fungi, or that another root-specific CYP81F isoform is important for mediating microbe-triggered production of this modified IG in roots. The possible isoform candidates are CYP81F3, which catalyzes the respective I3G substitution and exhibits a root-specific expression pattern, and CYP81F1, the function of which remains unclear (Fig. 1) (Pfalz et al., 2011).

Besides the toxic end products, which may affect fungal growth, unstable aglycones formed during the myrosinase-mediated hydrolysis of glucosinolates can decompose to nitriles whose formation is supported by specifier proteins (Wittstock et al., 2016). Consequently, hydrolysis of I3M may lead to the formation of IAN, which can be further converted to IAA by the activity of NIT1-3 (Fig. 1) (Janowitz et al., 2009; Lehmann et al., 2017). We initially hypothesized that *Ct*-induced PGP in *Arabidopsis* may be linked to changes in auxin signaling. As indicated by our analysis of *DR5::GUS* plants, Pi starvation reduced auxin levels, and this was at least partially restored upon *Ct* colonization (Fig. 3). Combining this observation with the earlier report on the requirement of PEN2 myrosinase for *Ct*-induced PGP (Hiruma et al., 2016), we hypothesized that PEN2-mediated IG hydrolysis contributes to IAA biosynthesis. However, $\Delta NIT2/NIT1/NIT3$ and *NIT2 RNAi* lines did not reveal defects in PGP, suggesting that either the observed *Ct*-mediated changes in auxin accumulation originate from another source, or that these changes are dispensable for the *Ct*-induced PGP. This also indicated that the impact of PEN2 on the PGP, as well as on pathogen biomass, stem from its role in the formation of glucosinolate catabolic products other than IAA. The changes in auxin signaling observed during the interaction with *Ct* could be due to canonical IAA biosynthesis, or due to the pathway that involves indole-3-acetamide hydrolase AMI1 and has been hypothesized to branch from IAOx (Lehmann et al., 2010; Mano and Nemoto, 2012). However, many pathogenic and endophytic microorganisms produce plant hormones, or their functional analogues, to manipulate host metabolic status

to their advantage (Chanclud and Morel, 2016). A few *Colletotrichum* spp. have also been shown to be capable of producing IAA (Robinson et al., 1998; Lu et al., 2000; Maor et al., 2004; Numponsak et al., 2018). To test whether *Ct* has this ability, we performed liquid chromatography-mass spectrometry analysis of extracts prepared from *Ct* hyphae, cultivated on potato dextrose agar (not shown). This did not reveal IAA production, but it cannot be excluded that *Ct* is able to synthesize IAA under different growth conditions, e.g. *in planta*. Overall, we cannot conclude at present whether the observed changes in auxin accumulation are related to IAA pools produced by the plant or by the fungus.

Our gene expression analysis revealed strong induction of *PR1* and *PDF1.2* transcription in *Ct*-colonized plants at all tested Pi concentrations (Fig. 6GH). These transcriptional changes suggest that, in addition to IG metabolism, colonization of *Arabidopsis* with *Ct* triggers other immune pathways including those dependent on SA and ethylene signaling. Notably, the expression of *PR1* and *PDF1.2* remained below the detection level in roots under similar experimental conditions (Hacquard et al., 2016), indicating that the changes observed here in the expression of both genes occur in leaves. This may explain why, as the WT-like PGP in the *ein2 sid2 dde2 pad4* quadruple mutant indicates, hormone signaling pathways are not crucial in controlling the interaction between *Arabidopsis* and *Ct*, which predominantly colonizes roots (Hiruma et al., 2016). In contrast to SA and ethylene pathways, expression levels of *VSP2* (Fig. 6I) indicated that depending on the Pi supply levels, JA-signaling is either not affected or even suppressed in the presence of *Ct*, which is in accordance with crosstalk between these pathways limiting fitness costs associated with defense (Vos et al., 2015). Constantly elevated *VSP2* expression at 100 and 50 μ M Pi indicated that, consistent with an earlier report, JA-dependent defense pathways are constitutively activated under Pi-starvation, which in turn may affect the interaction of plants with other organisms (Khan et al., 2016). The JA hormone is usually considered to be important in plant defenses against herbivores, but not against microbial pathogens. However, mutation in the JA-activated MYC2 transcription factor releases the JA-dependent repression of ETHYLENE RESPONSE FACTOR1, which is positively regulated by ethylene, leading to higher expression of *PDF1-2* and a higher resistance against necrotrophic pathogens, as shown for *Botrytis cinerea* (Song et al., 2014; Cagnola et al., 2018). To examine if lack of functional MYC2 could also affect interaction with beneficial microbes, we analyzed *Ct* biomass in the *myc2* mutant grown on 625 and 100 μ M Pi (Supplementary Fig. S5). We did not observe any impact of *myc2* mutation on *Ct* growth at high Pi, but at 100 μ M Pi fungal growth in *myc2* plants was reduced compared to WT plants. This indicates similar contributions of the MYC2-dependent branch of JA signaling to interactions with necrotrophic pathogens and beneficial fungi under low Pi supply.

Materials and methods

Arabidopsis loss-of-function and gain-of-function mutants used in this study

The *A. thaliana* loss-of-function and gain-of-function mutants used in this study are all in the Columbia-0 (Col-0) genetic background. Most loss-of-function mutants have already been described: *cyp79B2/B3* (Zhao et al., 2002), *pen2-2* (Lipka et al., 2005), *myb-tr* (Frerigmann and Gigolashvili, 2014a), *myc2/jin1.9* (Dombrecht et al., 2007). *NIT2-RNAi* was described by Lehmann et al. (2017) and *DR5::GUS* (Ulmasov et al., 1997). The Δ *NIT2/1/3* line was generated by CRISPR/Cas9, as described below.

Generation of Δ *NIT2/1/3* deletion plants by CRISPR/Cas9

The CRISPR/Cas9 construct for the deletion of the *NIT2/NIT1/NIT3* gene cluster on *A. thaliana* chromosome 3 was made in pKSE401 (Lowder et al., 2015). The target sequence (underlined) TGCTATTTGCTGGGAGAATAGG (the last three bases represent the PAM site) is located at the 3' end of exon 3 in all three *NIT1*-homologues, and contains the coding sequence for the catalytically active cysteine (Supplementary Fig. S6). Forward primer 5'ATTGTGCTATTTGCTGGGAGAAT3' and reverse primer 5'AAACATTCTCCCAGCAAATAGCA3' were hybridized to produce a double-stranded DNA with 5' ATTG- and AAAC overhangs, respectively, which was subsequently ligated into a BsaI-hydrolyzed pKSE401 plasmid, thereby removing a streptomycin resistance cassette and establishing a single-guide RNA containing the target sequence. The construct (pKSE401_NIT213_1) was verified by DNA sequencing.

Agrobacterium tumefaciens strain GV3101 was transformed with pKSE401_NIT213_1 by electroporation, and used for transformation of six individual plants of *A. thaliana* ecotype Col-0 by the floral-dip method (Clough and Bent, 1998). Kanamycin-resistant T1 plants (up to ten individuals of each transformed T0 plant) were tested for deletions within the *NIT2/NIT1/NIT3* gene cluster by PCR. Although some plants were positive for a *NIT2/NIT1/NIT3* deletion (as indicated by the occurrence of a short *NIT2-NIT3* PCR product; for primer sequences see Supplementary Table S1), these plants proved to be mosaic. T2 seedlings were pre-selected on Gamborg B5 medium containing 30 μ M indolacetonitrile (IAN), which allows for the screening of a non-functional *NIT1* gene: *nit1* plants are resistant against IAN, while wild-type (*NIT1*) plants show a typical auxin phenotype (Normanly et al., 1997). IAN-resistant plants were again analyzed by PCR and one plant was identified which was positive for a *NIT2/NIT1/NIT3* deletion, and in which none of the single *NIT1*, *NIT2* and *NIT3* genes could be amplified. Sequence analysis confirmed that the whole chromosomal fragment between the sites targeted by Cas9 cleavage in the *NIT2* and *NIT3* genes (~10,300 bases, including the last two exons of *NIT2* gene, the whole *NIT1* gene and the first three exons of the *NIT3* gene) was removed with the concomitant addition of a single

T residue (Supplementary Fig. S6B). The progeny of this plant (T3 generation) showed the same genotype, were resistant to IAN, showed no NIT1/NIT2/NIT3 protein by western blotting (Supplementary Fig. S6C), and no nitrilase activity with the substrate 6-heptenenitrile (Supplementary Fig. S6D). Resistance to IAN, western blotting and activity assays were performed as described in Lehmann et al. (2017).

Fungal co-cultivation with Arabidopsis

Three different media were used for co-cultivation of fungus with Arabidopsis, one with high phosphate (625 μM Pi), and two with low phosphate (100 μM /50 μM Pi). Agar plates were prepared with half-strength Murashige and Skoog (MS) medium (750 μM MgSO_4 , 625 μM KH_2PO_4 , 10.3 mM NH_4NO_3 , 9.4 mM KNO_3 , 1.5 mM CaCl_2 , 55 nM CoCl_2 , 53 nM CuCl_2 , 50 μM H_3BO_3 , 2.5 μM KI, 50 μM MnCl_2 , 520 nM Na_2MoO_4 , 15 μM ZnCl_2 , 75 μM Fe-EDTA, 500 μM MES-KOH pH 5.5) and supplemented with 1% Difco Agar Granulated (BD Biosciences, USA), an agar which contains limited amounts of bioavailable nutrients. Phosphate-depleted media was prepared according to a previous study (Gruber et al., 2013). After pouring the media into 120x120 mm square GREINER plates, a 2-cm slide was cut out of the plates.

C. tofieldiae fungus was grown on PDA-Media at 25 °C, at least for one day. The chambers were illuminated by three fluorescent lamps (MITSUBISHI/OSRAM FL40 SS W/37). Two sterile metal-beads were placed into 2-ml screw-lid tubes, then 100 mg of the fungus were excised with a sterile scalpel and added to the tubes. Excessive agar was removed by scratching off with the scalpel. This step secures a high concentration of the fungal material and ensures that the suspension is not viscous. Afterwards, 1 ml of 10 mM sterile MgCl_2 was added, and the tubes were shaken intensely for 10 minutes. After the homogenization, an additional 1 ml of MgCl_2 was added and the suspension was shaken again for 10 minutes. The final concentration of fungal material in the suspension was 50 mg/ml.

For the interaction experiment, stratified sterile Arabidopsis seeds were used. With a pipette and sterile tips, 20 μl fungal suspension (50 mg/ml) were added to 250 μl seeds in water for 5 minutes, and washed twice with 1 ml MgCl_2 (20 mM). By using a pipette with a cut sterile tip, the inoculated seeds were transferred to the low Pi and high Pi plates.

For each condition (high and low Pi), four to five replicate plates with seven seeds were prepared. The seeds were placed on the edge of the removed agar slide so that the cotyledons had enough space to grow without being inhibited by the agar. The seven seeds were placed at fixed distances to allow uninhibited growth. In addition to the fungal plates, mock plates (negative control) were prepared which contained only 10 mM MgCl_2 -washed seeds. These plates were compared to the fungal plates. To keep the plates sterile, 3M Micropore™ tape was used. Finally, the plates were moved to the phytochambers where

they were placed at a distance of one plate width from each other. Every four days, the plates were shuffled to simulate naturally fluctuating light conditions.

The plates with *Arabidopsis* plants/fungi were grown under short day conditions (10 hours at 21 °C and 14 hours at 19 °C). PANASONIC MLR-352-PE and SANYO MLR-351 were used as phytochambers. The chambers were illuminated by three lamps on each side (OSRAM L36W/965, OSRAM L36W/865 or FL40SS 40/37) with an illuminance of 11250 Lux +/- 4250 Lux.

RNA extraction and expression analysis by qRT-PCR

Total RNA extraction and qRT-PCR analysis were performed as described by (Frerigmann and Gigolashvili, 2014) using intact seedlings. The relative quantification of expression levels was performed using the comparative delta Ct method, and the calculated relative expression values were normalized to *PP2A* and compared with the expression level in untreated WT plants (Col-0 = 1). If not specified in the figure legend, three technical replicates, and three biological replicates from independently grown plants were analyzed (for primer sequences see Supplementary Table S2).

HPLC analysis of desulpho-GSL

The isolation and analysis of GSL content was performed using the desulpho-GSL method (Thies, 1979) on an ultra-performance liquid chromatography (UPLC) device (Waters, Eschborn), as described previously (Sewelam et al., 2014).

GUS assay

Entire seedlings were homogenized with a ball and 500 µl precooled extraction buffer (50 mM Na-Phosphate buffer (pH 7); 1 mM EDTA; 0.1 % (v/v) Triton X-100) for 2 min (20/s frequency), in a precooled TissueLyser. The crushed cells were centrifuged for 20 min at 4°C, and soluble proteins were isolated for determination of GUS activity using 4-methylumbelliferyl-β-D-glucuronide as a substrate. The amount of 4-methylumbelliferone formed was recorded fluorometrically (excitation, 340 nm; emission, 465 nm). For this, 200 µL of substrate buffer (protein extraction buffer with 1 mM 4-methylumbelliferyl-β-D-glucuronide), and 25 µL of protein extract were mixed, incubated at 37 °C in the dark, and measured every 10 to 30 min on a multi-well plate reader. The slope of the increase in 4-methylumbelliferone was determined in the linear range and divided by the amount of protein.

Acknowledgements

This work was supported by funding from the Max Planck Society (P.S.-L.), European Research Council advanced grant ROOTMICROBIOTA (P.S.-L.), Germany's Excellence Strategy CEPLAS (EXC-2048/1, Project 390686111) (P.S.-L.), and by the National Science Centre HARMONIA grant (UMO-2015/18/M/NZ1/00406) to P.B.

Figure legends

Figure 1. Biosynthetic links between Trp-derived specialized metabolites and IAA formation

MYB34/MYB51/MYB122-dependent effect on IG-related indolic compounds. The figure illustrates the direct regulatory impact of the three HIG-MYB transcription factors (TFs) (dotted lines) on the biosynthesis of related indolic compounds. Solid lines indicate single enzymatic steps, whereas dashed arrows stand for several enzymatic steps. IAOx, indole-3-acetaldoxime; IAN, indole-3-acetonitrile; IAA, indole-3-acetic acid; ICHO, indole-3-carbaldehyde; ICA, indole-3-carboxylic acid; DHCA, R-dihydro-camalexic acid; 4HO-ICN, 4-hydroxyindole-3-carbonyl nitrile; I3M, indole-3-methyl-GSL; 1HO-I3M, 1-hydroxy-I3M; 1MO-I3M, 1-methoxy-I3M; 4HO-I3M, 4-hydroxy-I3M; 4MO-I3M, 4-methoxy-I3M, RA, raphanusamic acid, I3A indole-3-methylamine.

Figure 2. *C. tofieldiae*-mediated growth promotion is sensitive to phosphate levels

Fresh weight (**A**) and root length (**B**) of *A. thaliana*. Results are means \pm SE from four independent experiments, each containing four replicate plates with seven seeds per plate ($n = 110$). Values marked with different letters are significantly different to each other (Kruskal-Wallis test with Bonferroni-corrected p -values; $p < 0.05$).

Figure 3. *C. tofieldiae* is able to restore auxin accumulation upon phosphate starvation

Results are means \pm SE from four independent experiments each containing three to four biological replicates ($n = 15$). Values marked with different letters are significantly different to each other (Kruskal-Wallis test with Bonferroni-corrected p -values; $p < 0.05$).

Figure 4. Diverse mutants in tryptophan-derived secondary metabolite metabolism show specific impairment of *C. tofieldiae*-mediated plant growth promotion

Root length (**A and B**) and fresh weight (**C and D**). Results are means \pm SE from three independent experiments containing four replicate plates each ($n = 42$). Values marked with asterisks are significantly different from respective Col-0 (Student's t -test; $p < 0.05$).

Figure 5. Nitrilase mutants show no impairment in *C. tofieldiae*-mediated PGP

Fungal growth **(A)** and dry weight per plate **(B)**. Results are means \pm SE from three independent experiments containing three or four replicates each (A; n = 9 /B; n = 12).. Values marked with asterisks are significantly different from respective Col-0 (Student's t-test; $p < 0.05$).

Figure 6. Co-cultivation with *C. tofieldiae* reverts PSR-mediated responses

Relative expression of selected genes measured in samples prepared from intact seedlings. Presented results are means \pm SE from three independent experiments, each containing three biological replicates (n = 9). Values marked with asterisks are significantly different from respective Col-0. Differences between MOCK and *C. tofieldiae* co-cultivation at specific phosphate concentrations are also indicated with asterisks (Student's t-test; $p < 0.05$).

Figure 7. Specific effects of *C. tofieldiae* co-cultivation on glucosinolate accumulation at different phosphate concentrations

Results are means \pm SE from four **(A/B)**/three **(C/D)** independent biological replicates (n = 16/9). Values marked with different letters are significantly different to each other (Kruskal-Wallis test with Bonferroni-corrected p -values; $p < 0.05$).

Supplementary Figure captions

Supplementary Figure 1. Higher fungal growth at lower phosphate concentrations.

Presented results are means \pm SE from one experiment with three biological replicates (n = 3). Values marked with asterisks are significantly different from Col-0 at full phosphate nutrition (Student's t-test; $p < 0.05$).

Supplementary Figure 2. Light- and *C. tofieldiae*-dependent effects on plant growth.

Presented results are means \pm SE from one experiment containing four replicate plates, with seven seeds per plate (n = 22). Values marked with asterisks are significantly different from respective Col-0 at full phosphate nutrition (Student's t-test; $p < 0.05$).

Low light conditions (1 lamp = 3600 Lux \pm 1370 Lux)

Medium light conditions (2 lamps = 6800 Lux \pm 2500 Lux)

High light conditions (3 lamps = 11250 Lux \pm 4250 Lux)

Supplementary Figure 3. Combination of phosphate starvation and *C. tofieldiae* cocultivation increases root hair number and length.

Supplementary Figure 4. Co-cultivation with *C. tofieldiae* reverts PSR-mediated anthocyanin accumulation.

Methanol-extracted anthocyanins from shoots bound on DEAE columns show a blue appearance. The pictures show four columns each from one representative experiment. Four independent experiments have been performed with similar results.

Supplementary Figure 5. MYC2 mutation diminishes fungal growth at lower phosphate concentrations.

The presented results are means \pm SE from one experiment with three biological replicates ($n = 3$). Values marked with asterisks are significantly different from respective Col-0 (Student's t-test; $p < 0.05$).

Supplementary Figure 6. Generation and characterization of $\Delta NIT2/NIT1/NIT3$ plants.

(A) The *NIT2/NIT1/NIT3* locus on chromosome 3. UTRs and introns are indicated by gray and black blocks, respectively. The targeted sequence for CRISPR/Cas is identical in all three genes, and contains the coding sequence for the catalytically active cysteine. (B) The final mutant has a deletion of approx. 10,3 kbp, ranging from exon 3 of *NIT2* to exon 3 of *NIT3*. The additional insertion of a single T residue results in a premature stop codon at the fusion site. The partial sequence alignment demonstrates the direct transition from the *NIT2* gene to the *NIT3* gene. (C) Coomassie-stained gel (upper panel), and western blot (lower panel) of protein extracts from wild type (WT), *NIT2 RNAi* and $\Delta NIT2/1/3$ plants. A 12.5% polyacrylamide gel was used to separate 50 μ g of total soluble protein. (D) Nitrilase activity assay using 6-heptenenitrile as substrate and 100 μ g total soluble protein from WT (squares) and $\Delta NIT2/1/3$ (circles) plants. Specific nitrilase activity was 176 ± 88 pkat mg^{-1} protein for the WT plants; no activity was detectable in the mutant plants.

Literature cited

- Bates, T.R., and Lynch, J.P. 1996. Stimulation of root hair elongation in *Arabidopsis thaliana* by low phosphorus availability. *Plant, Cell Environ.* 19:529-538.
- Bednarek, P., Pislewski-Bednarek, M., Svatos, A., Schneider, B., Doubsky, J., Mansurova, M., Humphry, M., Consonni, C., Panstruga, R., Sanchez-Vallet, A., Molina, A., and Schulze-Lefert, P. 2009. A glucosinolate metabolism pathway in living plant cells mediates broad-spectrum antifungal defense. *Science* 323:101-106.
- Böttcher, C., Chapman, A., Fellermeier, F., Choudhary, M., Scheel, D., and Glawischnig, E. 2014. The biosynthetic pathway of indole-3-carbaldehyde and indole-3-carboxylic acid derivatives in *Arabidopsis*. *Plant Physiol.* 165:841-853.

- Cagnola, J.I., Cerdán, P.D., Pacín, M., Andrade, A., Rodriguez, V., Zurbriggen, M.D., Legris, M., Buchovsky, S., Carrillo, N., Chory, J., Blázquez, M.A., Alabadi, D., and Casal, J.J. 2018. Long-day photoperiod enhances jasmonic acid-related plant defense. *Plant Physiol.* 178:163-173.
- Chanclud, E., and Morel, J.B. 2016. Plant hormones: A fungal point of view. *Mol. Plant Pathol.* 17:1289-1297.
- Chien, P.S., Chiang, C.P., Leong, S.J., and Chiou, T.J. 2018. Sensing and signaling of phosphate starvation: From local to long distance. *Plant Cell Physiol.* 59:1714-1722.
- Clay, N.K., Adio, A.M., Denoux, C., Jander, G., and Ausubel, F.M. 2009. Glucosinolate metabolites required for an *Arabidopsis* innate immune response. *Science* 323:95-101.
- Clough, S.J., and Bent, A.F. 1998. Floral dip: A simplified method for *Agrobacterium*-mediated transformation of *Arabidopsis thaliana*. *Plant J.* 16:735-743.
- Cosme, M., Fernández, I., Van der Heijden, M.G.A., and Pieterse, C.M.J. 2018. Non-mycorrhizal plants: The exceptions that prove the rule. *Trends Plant Sci.* 23:577-587.
- Crombez, H., Motte, H., and Beeckman, T. 2019. Tackling plant phosphate starvation by the roots. *Dev. Cell* 48:599-615.
- Díaz-González, S., Marín, P., Sánchez, R., Arribas, C., Kruse, J., González-Melendi, P., Brunner, F., and Sacristán, S. 2020. Mutualistic fungal endophyte *Colletotrichum tofieldiae* Ct0861 colonizes and increases growth and yield of maize and tomato plants. *Agronomy* 10:1493.
- Dombrecht, B., Xue, G.P., Sprague, S.J., Kirkegaard, J.A., Ross, J.J., Reid, J.B., Fitt, G.P., Sewelam, N., Schenk, P.M., and Manners, J.M. 2007. MYC2 differentially modulates diverse jasmonate-dependent functions in *Arabidopsis*. *Plant Cell* 19:2225–2245.
- Franco-Zorrilla, J.M., Valli, A., Todesco, M., Mateos, I., Puga, M.I., Rubio-Somoza, I., Leyva, A., Weigel, D., Garcia, J.A., and Paz-Ares, J. 2007. Target mimicry provides a new mechanism for regulation of microRNA activity. *Nat. Genet.* 39:1033-1037.
- Frerigmann, H., and Gigolashvili, T. 2014. Update on the role of R2R3-MYBs in the regulation of glucosinolates upon sulfur deficiency. *Front. Plant Sci.* 5:626.
- Frerigmann, H., and Gigolashvili, T. 2014a. MYB34, MYB51 and MYB122 Distinctly regulate indolic glucosinolate biosynthesis in *Arabidopsis thaliana*. *Mol. Plant* 7:814-828.
- Fujii, H., Chiou, T.J., Lin, S.I., Aung, K., and Zhu, J.K. 2005. A miRNA involved in phosphate-starvation response in *Arabidopsis*. *Curr. Biol.* 15:2038-2043.
- Glawischnig, E., Hansen, B.G., Olsen, C.E., and Halkier, B.A. 2004. Camalexin is synthesized from indole-3-acetaldoxime, a key branching point between primary and secondary metabolism in *Arabidopsis*. *Proc. Natl. Acad. Sci. USA* 101:8245-8250.

- Gruber, B.D., Giehl, R.F.H., Friedel, S., and von Wirén, N. 2013. Plasticity of the *Arabidopsis* root system under nutrient deficiencies. *Plant Physiol.* 163:161-179.
- Hacquard, S., Kracher, B., Hiruma, K., Münch, P.C., Garrido-Oter, R., Thon, M.R., Weimann, A., Damm, U., Dallery, J.-F., Hainaut, M., Henrissat, B., Lespinet, O., Sacristán, S., Ver Loren van Themaat, E., Kemen, E., McHardy, A.C., Schulze-Lefert, P., and O'Connell, R.J. 2016. Survival trade-offs in plant roots during colonization by closely related beneficial and pathogenic fungi. *Nat. Commun.* 7:11362.
- Halkier, B.A., and Gershenzon, J. 2006. Biology and biochemistry of glucosinolates. *Annu. Rev. Plant Biol.* 57:303-333.
- Hillebrand, H., Bartling, D., and Weiler, E.W. 1998. Structural analysis of the *nit2/nit1/nit3* gene cluster encoding nitrilases, enzymes catalyzing the terminal activation step in indole-acetic acid biosynthesis in *Arabidopsis thaliana*. *Plant Mol. Biol.* 36:89-99.
- Hiruma, K., Fukunaga, S., Bednarek, P., Piślewska-Bednarek, M., Watanabe, S., Narusaka, Y., Shirasu, K., and Takano, Y. 2013. Glutathione and tryptophan metabolism are required for *Arabidopsis* immunity during the hypersensitive response to hemibiotrophs. *Proc. Natl. Acad. Sci. USA* 110:9589-9594.
- Hiruma, K., Gerlach, N., Sacristán, S., Nakano, Ryohei T., Hacquard, S., Kracher, B., Neumann, U., Ramírez, D., Bucher, M., O'Connell, Richard J., and Schulze-Lefert, P. 2016. Root endophyte *Colletotrichum tofieldiae* confers plant fitness benefits that are phosphate status dependent. *Cell* 165:464-474.
- Hopkins, R.J., van Dam, N.M., and van Loon, J.J.A. 2009. Role of glucosinolates in insect-plant relationships and multitrophic interactions. *Annu. Rev. Entomol.* 54:57-83.
- Janowitz, T., Trompetter, I., and Piotrowski, M. 2009. Evolution of nitrilases in glucosinolate-containing plants. *Phytochemistry* 70:1680-1686.
- Khan, G.A., Vogiatzaki, E., Glauser, G., and Poirier, Y. 2016. Phosphate deficiency induces the jasmonate pathway and enhances resistance to insect herbivory. *Plant Physiol.* 171:632-644.
- Lahrmann, U., Strehmel, N., Langen, G., Frerigmann, H., Leson, L., Ding, Y., Scheel, D., Herklotz, S., Hilbert, M., and Zuccaro, A. 2015. Mutualistic root endophytism is not associated with the reduction of saprotrophic traits and requires a noncompromised plant innate immunity. *New Phytol.* 207:841-857.
- Lehmann, T., Hoffmann, M., Hentrich, M., and Pollmann, S. 2010. Indole-3-acetamide-dependent auxin biosynthesis: A widely distributed way of indole-3-acetic acid production? *Eur. J. Cell Biol.* 89:895-905.
- Lehmann, T., Janowitz, T., Sanchez-Parra, B., Alonso, M.M.P., Trompetter, I., Piotrowski, M., and Pollmann, S. 2017. *Arabidopsis* NITRILASE 1 contributes to the regulation of root

- growth and development through modulation of auxin biosynthesis in seedlings. *Front. Plant Sci.* 8:15.
- Lei, M.G., Zhu, C.M., Liu, Y.D., Karthikeyan, A.S., Bressan, R.A., Raghothama, K.G., and Liu, D. 2011. Ethylene signalling is involved in regulation of phosphate starvation-induced gene expression and production of acid phosphatases and anthocyanin in *Arabidopsis*. *New Phytol.* 189:1084-1095.
- Lipka, V., Dittgen, J., Bednarek, P., Bhat, R., Wiermer, M., Stein, M., Landtag, J., Brandt, W., Rosahl, S., and Scheel, D. 2005. Pre-and postinvasion defenses both contribute to nonhost resistance in *Arabidopsis*. *Science* 310:1180-1183.
- Liu, Y., Ahn, J.-E., Datta, S., Salzman, R.A., Moon, J., Huyghues-Despointes, B., Pittendrigh, B., Murdock, L.L., Koiwa, H., and Zhu-Salzman, K. 2005. *Arabidopsis* vegetative storage protein is an anti-insect acid phosphatase. *Plant Physiol.* 139:1545-1556.
- Lowder, L.G., Zhang, D., Baltes, N.J., Paul, J.W., 3rd, Tang, X., Zheng, X., Voytas, D.F., Hsieh, T.F., Zhang, Y., and Qi, Y. 2015. A CRISPR/Cas9 toolbox for multiplexed plant genome editing and transcriptional regulation. *Plant Physiol.* 169:971-985.
- Lu, H., Zou, W.X., Meng, J.C., Hu, J., and Tan, R.X. 2000. New bioactive metabolites produced by *Colletotrichum* sp., an endophytic fungus in *Artemisia annua*. *Plant Sci.* 151:67-73.
- Malka, S.K., and Cheng, Y. 2017. Possible interactions between the biosynthetic pathways of indole glucosinolate and auxin. *Front. Plant Sci.* 8:2131.
- Mano, Y., and Nemoto, K. 2012. The pathway of auxin biosynthesis in plants. *J. Exp. Bot.* 63:2853-2872.
- Maor, R., Haskin, S., Levi-Kedmi, H., and Sharon, A. 2004. In planta production of indole-3-acetic acid by *Colletotrichum gloeosporioides* f. sp. *aeschynomene*. *Appl. Environ. Microbiol.* 70:1852-1854.
- Muchhal, U.S., Pardo, J.M., and Raghothama, K.G. 1996. Phosphate transporters from the higher plant *Arabidopsis thaliana*. *Proc. Natl. Acad. Sci. USA* 93:10519-10523.
- Nacry, P., Canivenc, G., Muller, B., Azmi, A., Van Onckelen, H., Rossignol, M., and Dumas, P. 2005. A Role for auxin redistribution in the responses of the root system architecture to phosphate starvation in *Arabidopsis*. *Plant Physiol.* 138:2061-2074.
- Normanly, J., Grisafi, P., Fink, G.R., and Bartel, B. 1997. *Arabidopsis* mutants resistant to the auxin effects of indole-3-acetonitrile are defective in the nitrilase encoded by the *NIT1* gene. *Plant Cell* 9:1781-1790.
- Numponsak, T., Kumla, J., Suwannarach, N., Matsui, K., and Lumyong, S. 2018. Biosynthetic pathway and optimal conditions for the production of indole-3-acetic acid by an endophytic fungus, *Colletotrichum fructicola* CMU-A109. *PLoS One* 13:e0205070.

- Pant, B.D., Pant, P., Erban, A., Huhman, D., Kopka, J., and Scheible, W.R. 2015. Identification of primary and secondary metabolites with phosphorus status-dependent abundance in *Arabidopsis*, and of the transcription factor PHR1 as a major regulator of metabolic changes during phosphorus limitation. *Plant, Cell Environ.* 38:172-187.
- Parniske, M. 2008. Arbuscular mycorrhiza: The mother of plant root endosymbioses. *Nat. Rev. Microbiol.* 6:763-775.
- Pastorczyk, M., and Bednarek, P. 2016. The Function of Glucosinolates and Related Metabolites in Plant Innate Immunity. *Adv. Bot. Res.* 80:171-198.
- Pastorczyk, M., Kosaka, A., Piślewska-Bednarek, M., López, G., Frerigmann, H., Kułak, K., Glawischnig, E., Molina, A., Takano, Y., and Bednarek, P. 2020. The role of CYP71A12 monooxygenase in pathogen-triggered tryptophan metabolism and *Arabidopsis* immunity. *New Phytol.* 225:400-412.
- Péret, B., Clément, M., Nussaume, L., and Desnos, T. 2011. Root developmental adaptation to phosphate starvation: better safe than sorry. *Trends Plant Sci.* 16:442-450.
- Pérez-Torres, C.-A., López-Bucio, J., Cruz-Ramírez, A., Ibarra-Laclette, E., Dharmasiri, S., Estelle, M., and Herrera-Estrella, L. 2008. Phosphate availability alters lateral root development in *Arabidopsis* by modulating auxin sensitivity via a mechanism involving the TIR1 auxin receptor. *Plant Cell* 20:3258-3272.
- Pfalz, M., Mikkelsen, M.D., Bednarek, P., Olsen, C.E., Halkier, B.A., and Kroymann, J. 2011. Metabolic engineering in *Nicotiana benthamiana* reveals key enzyme functions in *Arabidopsis* indole glucosinolate modification. *Plant Cell* 23:716-729.
- Prerostova, S., Kramna, B., Dobrev, P.I., Gaudinova, A., Marsik, P., Fiala, R., Knirsch, V., Vanek, T., Kuresova, G., and Vankova, R. 2018. Organ-specific hormonal cross-talk in phosphate deficiency. *Environ. Exp. Bot.* 153:198-208.
- Robinson, M., Riov, J., and Sharon, A. 1998. Indole-3-acetic acid biosynthesis in *Colletotrichum gloeosporioides* f. sp. *aeschynomene*. *Appl. Environ. Microbiol.* 64:5030-5032.
- Sanchez-Vallet, A., Ramos, B., Bednarek, P., Lopez, G., Pislewska-Bednarek, M., Schulze-Lefert, P., and Molina, A. 2010. Tryptophan-derived secondary metabolites in *Arabidopsis thaliana* confer non-host resistance to necrotrophic *Plectosphaerella cucumerina* fungi. *Plant J.* 63:115-127.
- Sewelam, N., Jaspert, N., Van Der Kelen, K., Tognetti, V.B., Schmitz, J., Frerigmann, H., Stahl, E., Zeier, J., Van Breusegem, F., and Maurino, V.G. 2014. Spatial H₂O₂ signalling specificity: H₂O₂ from chloroplasts and peroxisomes modulates the plant transcriptome differentially. *Mol. Plant* 7:1191-1210.

- Song, S., Huang, H., Gao, H., Wang, J., Wu, D., Liu, X., Yang, S., Zhai, Q., Li, C., Qi, T., and Xie, D. 2014. Interaction between MYC2 and ETHYLENE INSENSITIVE3 modulates antagonism between jasmonate and ethylene signaling in *Arabidopsis*. *Plant Cell* 26:263-279.
- Thies, W. 1979. Detection and utilization of a glucosinolate sulfohydrolase in the edible snail, *Helix pomatia*. *Naturwissenschaften* 66:364-365.
- Ulmasov, T., Murfett, J., Hagen, G., and Guilfoyle, T.J. 1997. Aux/IAA proteins repress expression of reporter genes containing natural and highly active synthetic auxin response elements. *Plant Cell* 9:1963-1971.
- Vorwerk, S., Biernacki, S., Hillebrand, H., Janzik, I., Müller, A., Weiler, E.W., and Piotrowski, M. 2001. Enzymatic characterization of the recombinant *Arabidopsis thaliana* nitrilase subfamily encoded by the *NIT2/NIT1/NIT3*-gene cluster. *Planta* 212:508-516.
- Vos, I.A., Moritz, L., Pieterse, C.M.J., and Van Wees, S.C.M. 2015. Impact of hormonal crosstalk on plant resistance and fitness under multi-attacker conditions. *Front. Plant Sci.* 6:639.
- Wittstock, U., Kurzbach, E., Herfurth, A.M., and Stauber, E.J. 2016. Glucosinolate Breakdown. *Adv. Bot. Res.* 80:125-169.
- Zarei, A., Korbes, A.P., Younessi, P., Montiel, G., Champion, A., and Memelink, J. 2011. Two GCC boxes and AP2/ERF-domain transcription factor ORA59 in jasmonate/ethylene-mediated activation of the *PDF1.2* promoter in *Arabidopsis*. *Plant Mol. Biol.* 75:321-331.
- Zhao, Y., Hull, A.K., Gupta, N.R., Goss, K.A., Alonso, J., Ecker, J.R., Normanly, J., Chory, J., and Celenza, J.L. 2002. Trp-dependent auxin biosynthesis in *Arabidopsis*: Involvement of cytochrome P450s CYP79B2 and CYP79B3. *Genes Dev.* 16:3100-3012.

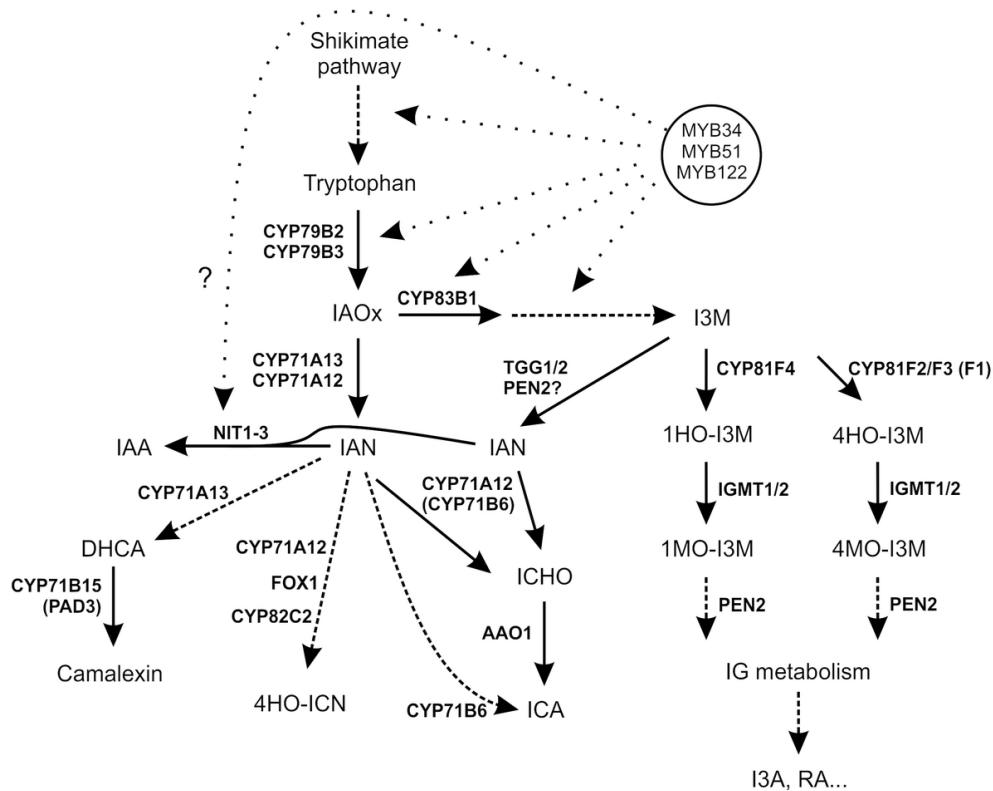


Figure 1. Biosynthetic links between Trp-derived specialized metabolites and IAA formation. MYB34/MYB51/MYB122-dependent effect on IG-related indolic compounds. The figure illustrates the direct regulatory impact of the three HIG-MYB transcription factors (TFs) (dotted lines) on the biosynthesis of related indolic compounds. Solid lines indicate single enzymatic steps, whereas dashed arrows stand for several enzymatic steps. IAox, indole-3-acetaldoxime; IAN, indole-3-acetonitrile; IAA, indole-3-acetic acid; ICCHO, indole-3-carbaldehyde; ICA, indole-3-carboxylic acid; DHCA, R-dihydro-camalexenic acid; 4HO-ICN, 4-hydroxyindole-3-carbonyl nitrile; I3M, indole-3-methyl-GSL; 1HO-I3M, 1-hydroxy-I3M; 1MO-I3M, 1-methoxy-I3M; 4HO-I3M, 4-hydroxy-I3M; 4MO-I3M, 4-methoxy-I3M, RA, raphanusamic acid, I3A indole-3-methylamine.

102x81mm (300 x 300 DPI)

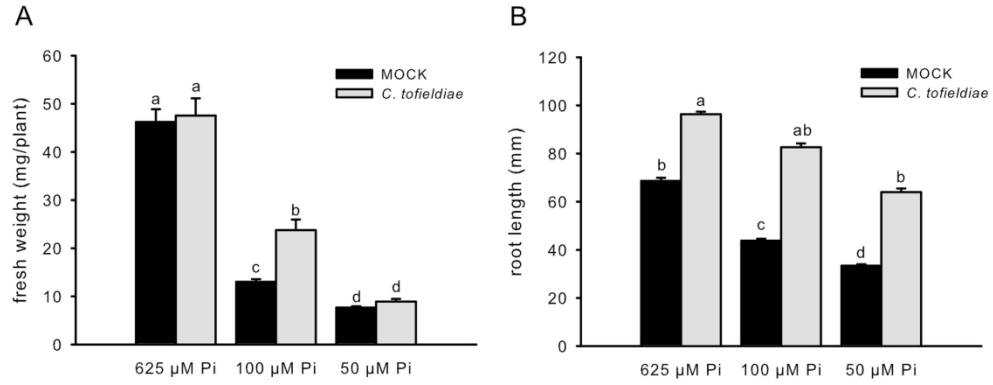


Figure 2. *C. tofieldiae*-mediated growth promotion is sensitive to phosphate levels Fresh weight (A) and root length (B) of *A. thaliana*. Results are means \pm SE from four independent experiments, each containing four replicate plates with seven seeds per plate ($n = 110$). Values marked with different letters are significantly different to each other (Kruskal-Wallis test with Bonferroni-corrected p-values; $p < 0.05$).

159x61mm (300 x 300 DPI)

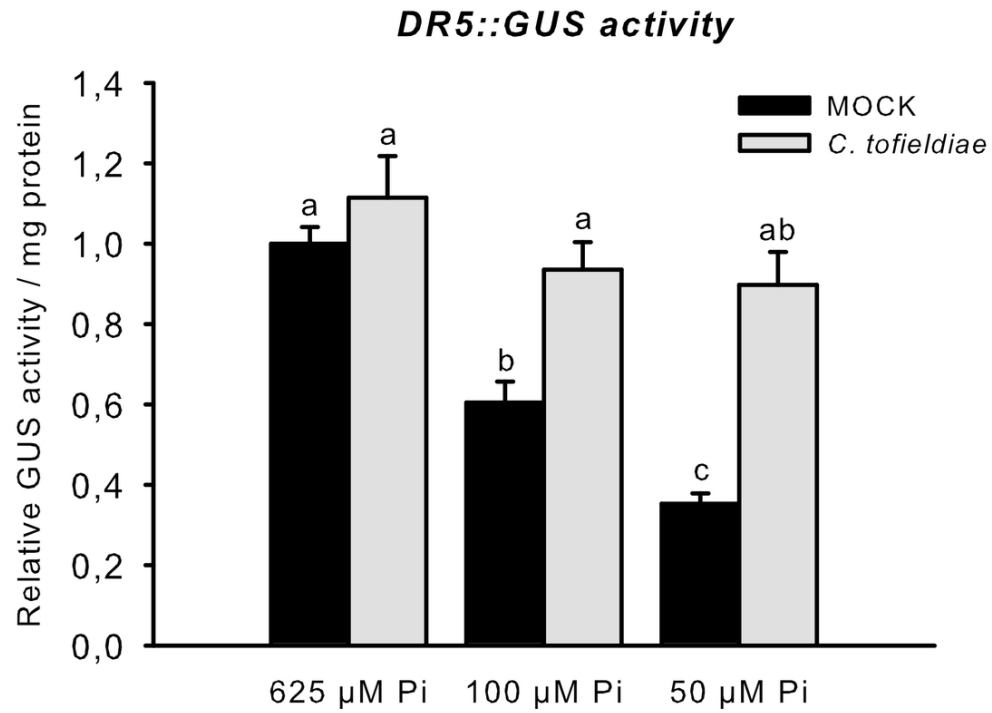


Figure 3. *C. tofieldiae* is able to restore auxin accumulation upon phosphate starvation. Results are means \pm SE from four independent experiments each containing three to four biological replicates ($n = 15$). Values marked with different letters are significantly different to each other (Kruskal-Wallis test with Bonferroni-corrected p -values; $p < 0.05$).

93x66mm (300 x 300 DPI)

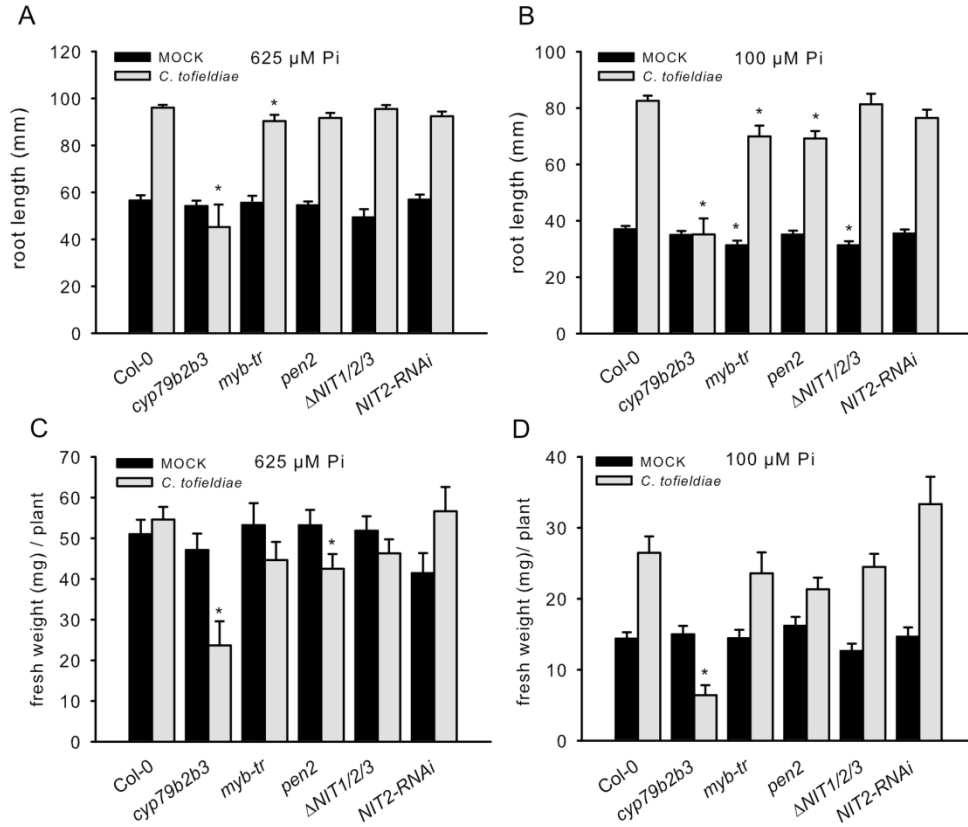


Figure 4. Diverse mutants in tryptophan-derived secondary metabolite metabolism show specific impairment of *C. tofieldiae*-mediated plant growth promotion. Root length (A and B) and fresh weight (C and D). Results are means \pm SE from three independent experiments containing four replicate plates each (n = 42). Values marked with asterisks are significantly different from respective Col-0 (Student's t-test; $p < 0.05$).

165x136mm (300 x 300 DPI)

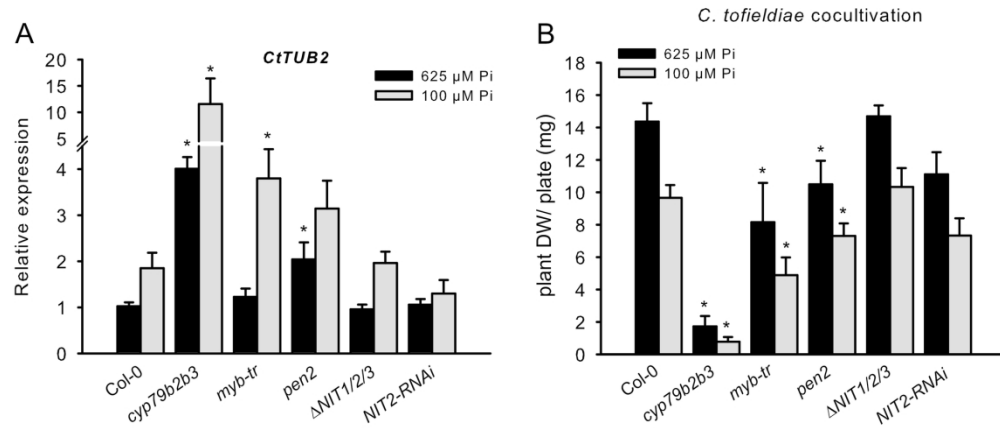


Figure 5. Nitrilase mutants show no impairment in *C. tofieldiae*-mediated PGP Fungal growth (A) and dry weight per plate (B). Results are means \pm SE from three independent experiments containing three or four replicates each (A; n = 9 / B; n = 12). Values marked with asterisks are significantly different from respective Col-0 (Student's t-test; $p < 0.05$).

177x78mm (300 x 300 DPI)

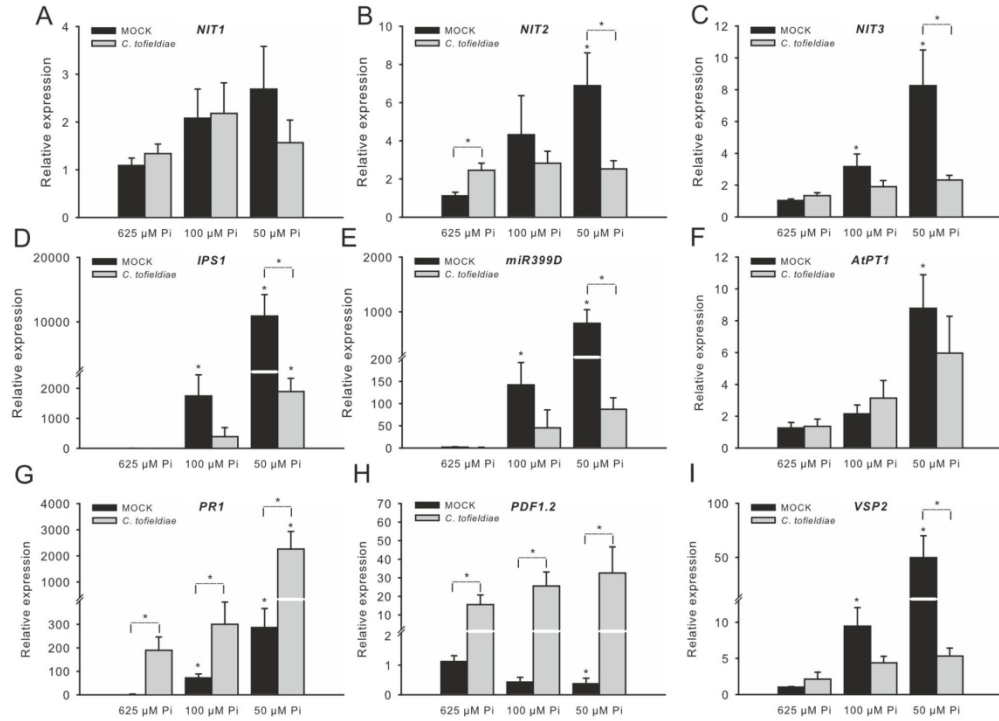


Figure 6. Co-cultivation with *C. tofieldiae* reverts PSR-mediated responses. Relative expression of selected genes measured in samples prepared from intact seedlings. Presented results are means \pm SE from three independent experiments, each containing three biological replicates ($n = 9$). Values marked with asterisks are significantly different from respective Col-0. Differences between MOCK and *C. tofieldiae* co-cultivation at specific phosphate concentrations are also indicated with asterisks (Student's t-test; $p < 0.05$).

160x115mm (300 x 300 DPI)

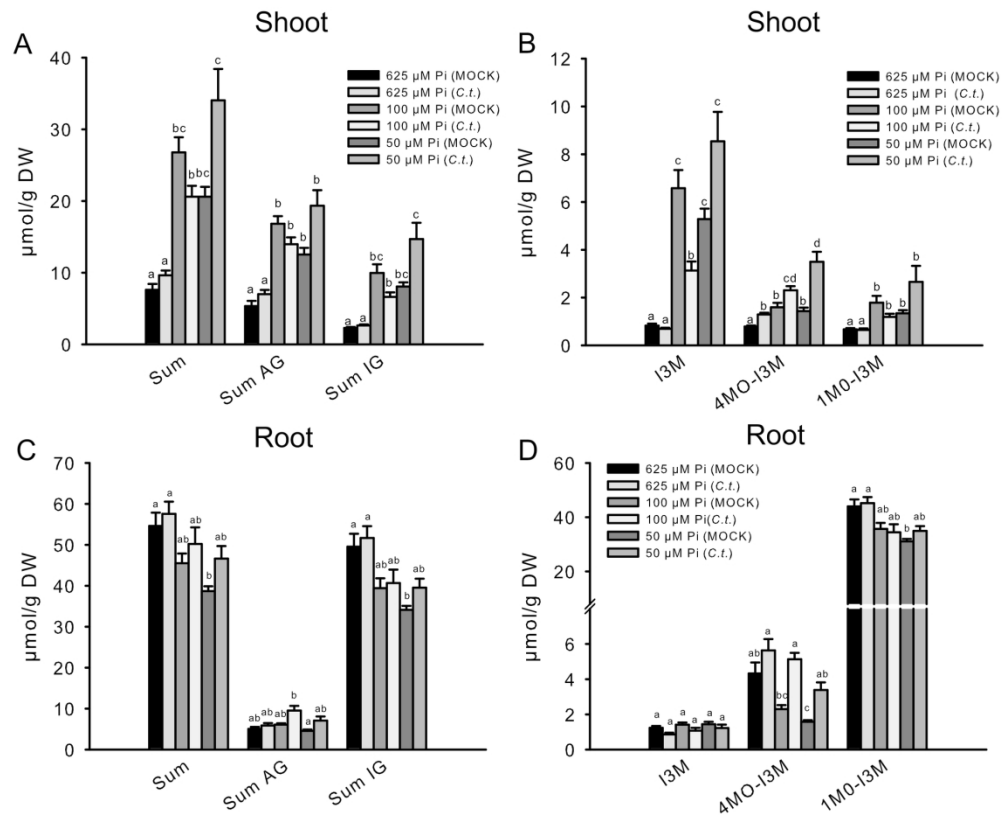


Figure 7. Specific effects of *C. tofieldiae* co-cultivation on glucosinolate accumulation at different phosphate concentrations. Results are means \pm SE from four (A/B)/three (C/D) independent biological replicates ($n = 16/9$). Values marked with different letters are significantly different to each other (Kruskal-Wallis test with Bonferroni-corrected p -values; $p < 0.05$).

176x143mm (300 x 300 DPI)

Supplementary materials

A network of phosphate starvation and immune-related signaling and metabolic pathways controls the interaction between *Arabidopsis thaliana* and the beneficial fungus *Colletotrichum tofieldiae*

Henning Frerigmann^{1,2}, Markus Piotrowski³, René Lemke³, Paweł Bednarek^{2*}, Paul Schulze-Lefert^{1*}

¹ Max Planck Institute for Plant Breeding Research, Department of Plant Microbe Interactions and Cluster of Excellence on Plant Sciences (CEPLAS), D-50829 Cologne, Germany

² Institute of Bioorganic Chemistry, Polish Academy of Sciences, 61-704 Poznań, Poland

³ Lehrstuhl für Molekulargenetik und Physiologie der Pflanzen, Ruhr-Universität Bochum, D-44801 Bochum, Germany

* Corresponding authors: schlef@mpipz.mpg.de; bednarek@ibch.poznan.pl

Supplementary Materials and Methods

Supplementary Figures 1-6

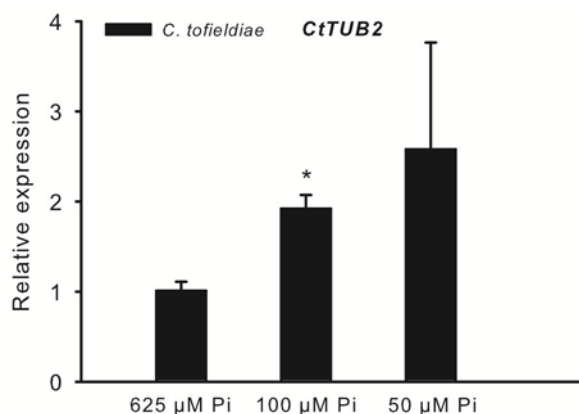
Supplementary Tables 1-2

Supplementary Materials and Methods

Semiquantitative analysis of anthocyanin levels

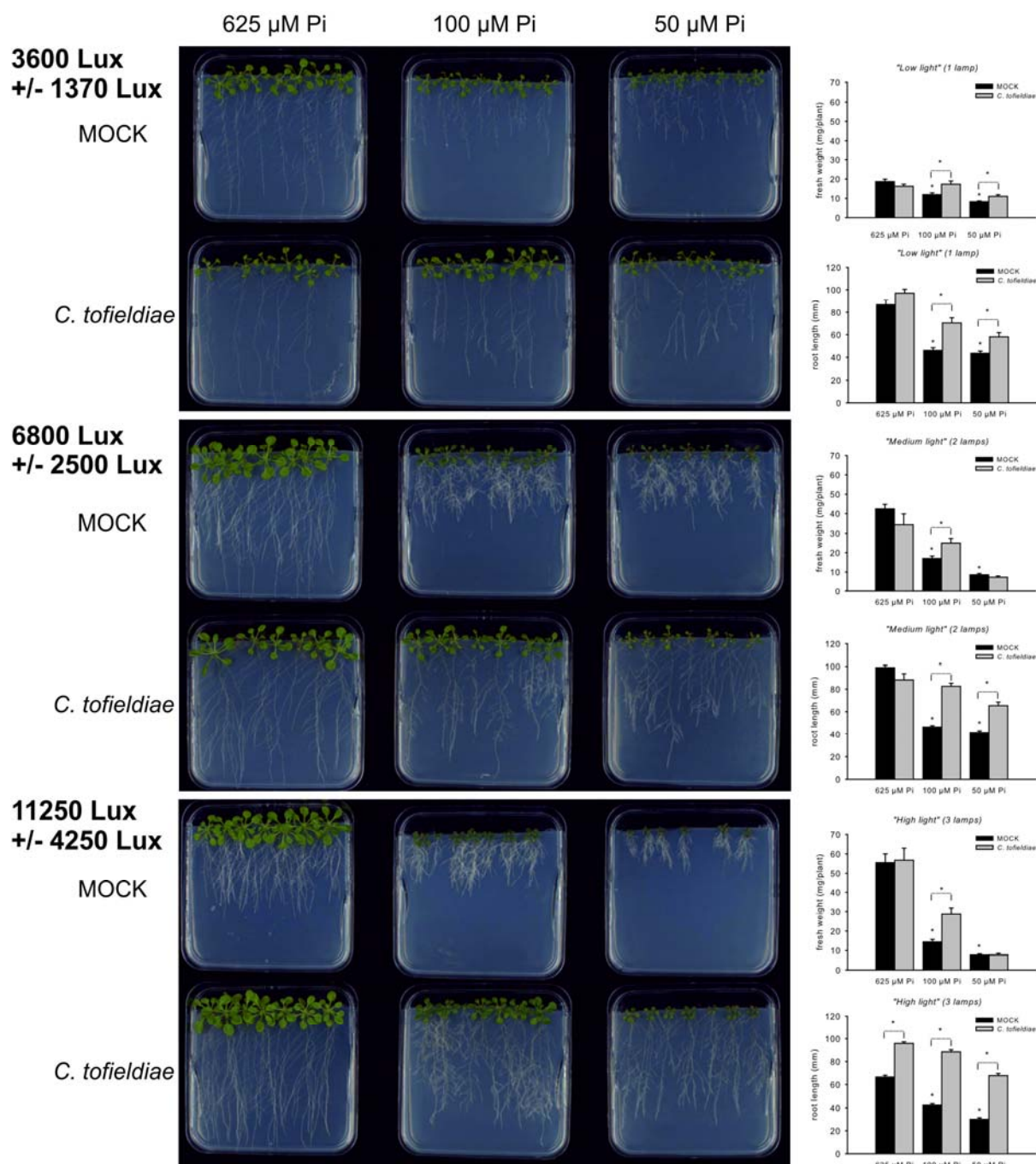
For qualitative analysis of anthocyanin levels, the shoot samples were lyophilized and ground to a fine powder with a metal bead in a ball mill. The anthocyanins were extracted with 1 ml 80% methanol. Extracts were loaded on a DEAE Sephadex column (0.1 g equilibrated in 0.5 M acetic acid/NaOH pH 5), washed first with 2 ml water and then with 4 ml 0.02 M acetic acid/NaOH buffer (pH 5). After overnight conversion of glucosinolates to desulfoglucosinolates by sulfatase from *Helix pomatia* (Thies, 1979) columns were washed with 6 ml water and pictures of column-bound anthocyanins were taken (Supplementary Fig. S4).

Supplementary Figures



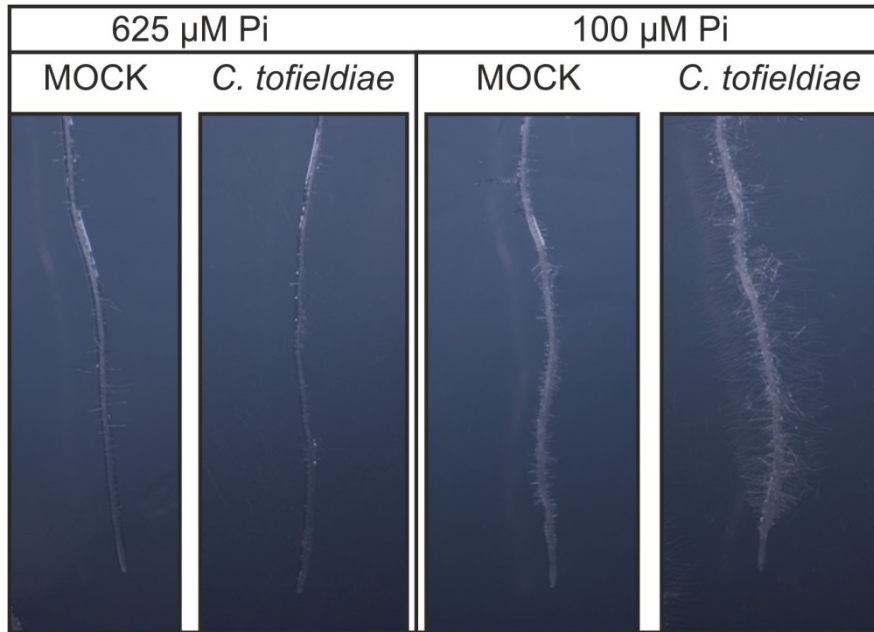
Supplementary Figure 1. Higher fungal growth at lower phosphate concentrations.

Presented results are means \pm SE from one experiment with three biological replicates ($n = 3$). Values marked with asterisks are significantly different from Col-0 at full phosphate nutrition (Student's t-test; $p < 0.05$).

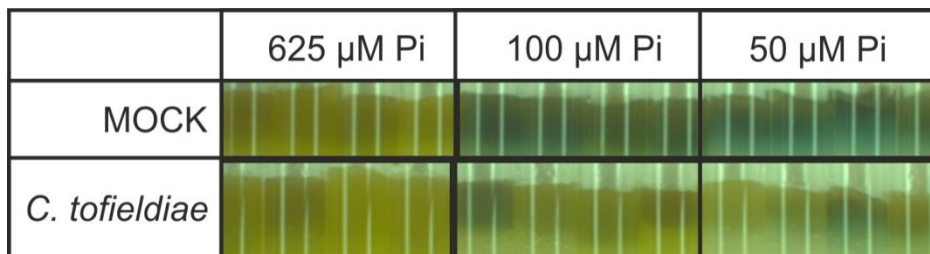


Supplementary Figure 2. Light- and *C. tofieldiae*-dependent effects on plant growth.

Presented results are means \pm SE from one experiment containing four replicate plates, with seven seeds per plate ($n = 22$). Values marked with asterisks are significantly different from respective Col-0 at full phosphate nutrition (Student's t-test; $p < 0.05$).

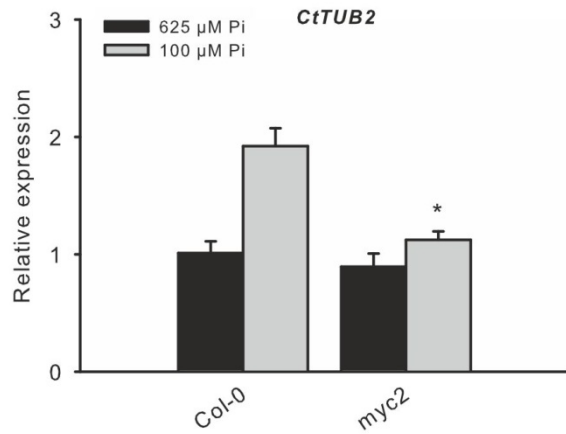


Supplementary Figure 3. Combination of phosphate starvation and *C. tofieldiae* cocultivation increases root hair number and length.



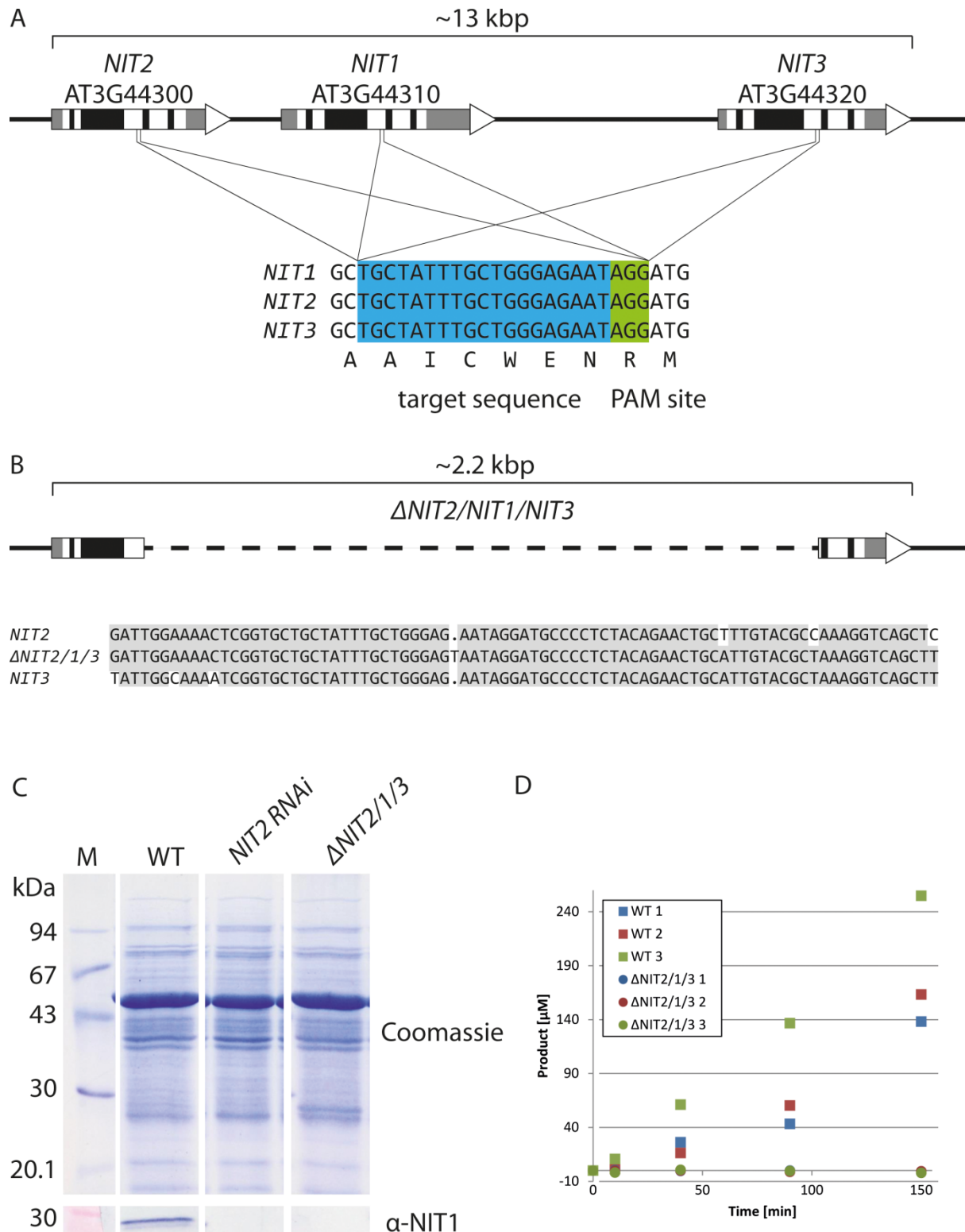
Supplementary Figure 4. Co-cultivation with *C. tofieldiae* reverts PSR-mediated anthocyanin accumulation.

Methanol-extracted anthocyanins from shoots bound on DEAE columns show a blue appearance. The pictures show four columns each from one representative experiment. Four independent experiments have been performed with similar results.



Supplementary Figure 5. MYC2 mutation diminishes fungal growth at lower phosphate concentrations.

The presented results are means \pm SE from one experiment with three biological replicates ($n = 3$). Values marked with asterisks are significantly different from respective Col-0 (Student's t-test; $p < 0.05$).



Supplementary Figure 6. Generation and characterization of Δ *NIT2/NIT1/NIT3* plants.

(A) The *NIT2/NIT1/NIT3* locus on chromosome 3. UTRs and introns are indicated by gray and black blocks, respectively. The targeted sequence for CRISPR/Cas is identical in all three genes, and contains the coding sequence for the catalytically active cysteine. (B) The final mutant has a deletion of approx. 10,3 kbp, ranging from exon 3 of *NIT2* to exon 3 of *NIT3*. The additional insertion of a single T residue results in a premature stop codon at the

fusion site. The partial sequence alignment demonstrates the direct transition from the *NIT2* gene to the *NIT3* gene. (C) Coomassie-stained gel (upper panel), and western blot (lower panel) of protein extracts from wild type (WT), *NIT2 RNAi* and $\Delta NIT2/1/3$ plants. A 12.5% polyacrylamide gel was used to separate 50 μg of total soluble protein. (D) Nitrilase activity assay using 6-heptenenitrile as substrate and 100 μg total soluble protein from WT (squares) and $\Delta NIT2/1/3$ (circles) plants. Specific nitrilase activity was 176 ± 88 pkat mg^{-1} protein for the WT plants; no activity was detectable in the mutant plants.

Supplementary Tables

Supplementary Table 1. Primer sequences for PCR analysis of Δ NIT2/1/3 plants.
Primers bind to the 2nd (Fw) and 3rd (Rv) intron of the respective genes, spanning exon 3.

Oligonucleotide name	AT-Number	Oligo Sequence 5'-3'
NIT1_In2_3_Fw	AT3G44310	TGGAACACAAAATGACTCTTTTTGG
NIT1_In2_3_Rv		AAAGCCTAGATGTTTCAAACGGC
NIT2_In2_3_Fw	AT3G44300	TTATATGGTACTTTTTTTGTGTGATGAACC
NIT2_In2_3_Rv		CAAACACTCAAATAAATTGCATCAAG
NIT3_In2_3_Fw	AT3G44320	CTTGCATATGTTTGGTACTCTTGTAATG
NIT3_In2_3_Rv		ACAAGCCGGATATGTCAAGCTAC

Supplementary Table 2. Primer sequences used in qPCR analysis.

Oligonucleotide name	AT-Number	Oligo Sequence 5'-3'
NIT1_RL_Fw	AT3G44310	AGTAGCAAGATTGGCTGACGTG
NIT1_RL_Rv		GGTATACCCTTCCTTCTCTATGGC
NIT2_RL_Fw	AT3G44300	GTAGAAAAGTTGGCGGAGTTGG
NIT2_RL_Rv		TGCTGTGCAATAGAGTGTATACCCA
NIT3_RL_Fw	AT3G44320	TCCGGAGGTGGAAGTGCATTATT
NIT3_RL_Rv		GGCTTTGAGTAATGTCCAACCACA
IPS1_RL_Fw	AT3G09922	AGACTGCAGAAGGCTGATTCAGA
IPS1_RL_Rv		TTGCCCAATTTCTAGAGGGAGA
miR399D_RL_Fw	At2G34202	AATACTCCTATGGCAGATCGCATTGG
miR399D_RL_Rv		TCCTTTGGCAGAGAAGCATTTTACTTG
AtPT1_RL_Fw	At5G43350	TGATGATCTTGTGCTCTGTGC
AtPT1_RL_Rv		ATGACACCCTTGGCTTCGT
PR1_RL_Fw	At2G14610	GTGCCAAAGTGAGGTGTAACAA
PR1_RL_Rv		CGTGTGTATGCATGATCACATC
PDF1.2a_RL_Fw	At5G44420	CCAAGTGGGACATGGTCAG
PDF1.2a_RL_Rv		ACTTGTGTGCTGGGAAGACA
VSP2_RL_Rv	AT5G24770	GGCACCGTGTGCGAAGTTTAT
VSP2_RL_Fw		CTCTTGGTCGCTACGGTCTC
PP2A_RL_Fw	At1G59830	CAAGAGGTTCCACACGAAGGA
PP2A_RL_Rv		TGTAACCAGCACACGAGGA
CtTUB2_RL_Fw	CT04_11973	AGTCTTTCCTGATCCCGACC
CtTUB2_RL_Rv		AAGTGGCCAGATCAAGTCAA.
At16S_RL_FW	AtCG00920	CAGGCGGTGGAAACTACCAAG
At16S_RL_Rv		TACAGCACTGCACGGGTCGAT